AGU PUBLICATIONS

Geophysical Research Letters

RESEARCH LETTER
10.1002/2014GL060249

Key Points:
- Narrow fronts form at the head or reconnection-driven outflows
- The front velocity is less than the bulk flow and acts to deflect the bulk flow
- The reflection of ions ahead of the front deflects and dissipates the bulk flow

Correspondence to:
J. F. Drake,
drake@umd.edu

Citation:
Drake, J. F., M. Swisdak, P. A. Cassak, and T. D. Phan (2014), On the 3-D structure and dissipation of reconnection-driven flow bursts, *Geophys. Res. Lett.*, *41*, 3710–3716, doi:10.1002/2014GL060249.

Received 15 APR 2014
Accepted 19 MAY 2014
Accepted article online 23 MAY 2014
Published online 3 JUN 2014

On the 3-D structure and dissipation of reconnection-driven flow bursts

J. F. Drake[1], M. Swisdak[2], P. A. Cassak[3], and T. D. Phan[4]

[1]Department of Physics and the Institute for Physical Sciences and Technology, University of Maryland, College Park, Maryland, USA, [2]Institute for Research in Electronics and Applied Physics, University of Maryland, College Park, Maryland, USA, [3]Department of Physics and Astronomy, West Virginia University, Morgantown, West Virginia, USA, [4]Space Science Laboratory, University of California, Berkeley, California, USA

Abstract The structure of magnetic reconnection-driven outflows and their dissipation are explored with 3-D particle-in-cell simulations. Outflow jets resulting from 3-D reconnection with a finite length x-line form fronts as they propagate into the downstream medium. A large pressure increase ahead of this "reconnection jet front" (RJF) due to reflected ions slows the front so that its velocity is well below that of the ambient ions in the core of the jet. As a result, the RJF slows and diverts the high-speed flow into the direction perpendicular to the reconnection plane. The RJF therefore acts as a thermalization site for the ion bulk flow and contributes significantly to the dissipation of magnetic energy during reconnection even though the outflow jet is subsonic. This behavior has no counterpart in 2-D reconnection. A simple analytic model predicts the front velocity and the fraction of the ion bulk flow energy that is dissipated.

Magnetic reconnection is the dominant mechanism for dissipating magnetic energy in large-scale plasma systems and is the driver of explosive events such as flares in astrophysical systems and flow bursts in the Earth's magnetosphere. Most of the energy released during reconnection takes place not at the x-line but downstream in the exhaust where newly reconnected field lines relax their magnetic tension. In the MHD description the Petschek shocks that bound the exhaust both drive the Alfvénic exhaust and heat the upstream plasma entering the exhaust [*Petschek*, 1964; *Lin and Lee*, 1995]. In the nearly collisionless environment of many systems, while the exhaust outflow is close to the MHD prediction [*Sonnerup et al.*, 1981], the exhaust heating results from counterstreaming ions [*Hoshino et al.*, 1998; *Gosling et al.*, 2005] rather than Petschek shocks. The kinetic energy of the bulk flow driven during reconnection is a substantial fraction of the released magnetic energy, and in natural systems this energy is ultimately dissipated. However, the dominant processes that control the dissipation of these flows and their universality have not yet been established.

During solar flares the termination shock that has been observed at the low-altitude edge of coronal reconnection exhausts [*Masuda et al.*, 1994] is a possible mechanism for the dissipation of the energy in the bulk flow. Supra-arcade downflows (SADs) [*McKenzie and Hudson*, 1999], which are believed to be driven by reconnection, are observed to slow during their downward trajectory toward the solar surface. In the Earth's magnetotail a key observational discovery was the formation of narrow boundary layers or fronts at the interface of the high-speed reconnection jets and the essentially stationary ambient plasma downstream. At the front the amplitude of the magnetic field normal to the initial current layer (B_z in the magnetotail) increases abruptly [*Ohtani et al.*, 2004; *Runov et al.*, 2009, 2011a]. Initially, such fronts (dubbed "dipolarization fronts") were believed to result from the slowing of the reconnection outflow as it impacted the strong dipole field of the Earth, similar to coronal termination shocks. However, the measured propagation of these fronts over large distances both earthward and tailward of the reconnection site [*Ohtani et al.*, 2004; *Angelopoulos et al.*, 2013] is strong evidence that these fronts are generically associated with the development of reconnection in natural systems and are not specific to the geometry of a particular system.

The role that reconnection jet fronts (RJFs) play is, however, unclear. It has been suggested that RJFs may be important sites for energy dissipation [*Hoshino et al.*, 2001; *Runov et al.*, 2011b; *Angelopoulos et al.*, 2013]. A number of 2-D reconnection simulations (corresponding to an infinite length x-line) have been carried out to explore the structure of RJFs [*Sitnov et al.*, 2009; *Wu and Shay*, 2012]. On the other hand, it is unlikely that reconnection in physical systems is 2-D since reconnection very likely onsets in a spatially localized region. Flow bursts and associated RJFs in the magnetotail are localized in the cross-tail (y) direction with

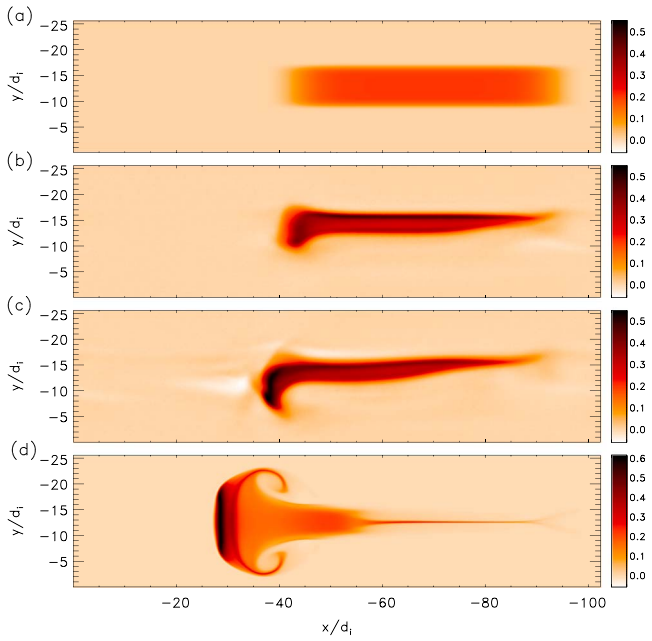

Figure 1. From the PIC simulation plots of B_z in the x-y plane at the center of the current sheet ($z = 0$) at (a) $t = 0$, (b) $t = 12\Omega_{ci}^{-1}$, and (c) $t = 24\Omega_{ci}^{-1}$. (d) A similar plot from an MHD simulation with nearly identical initial conditions at the same time as in Figure 1c.

characteristic scales of several Earth radii R_E [*Angelopoulos et al.*, 1997; *Nakamura et al.*, 2004] and therefore correspond to finite length x-lines. SADs have similarly been interpreted as resulting from reconnection with finite length x-lines [*Linton and Longcope*, 2006; *Cassak et al.*, 2013]. We show that the structure of the exhaust and its dissipation depends critically on its 3-D structure.

Since we are focusing on the structure of the reconnection outflows and the associated RJF and not on the structure of the dissipation region where field lines change topology, we explore the dynamics with the Riemann approach [*Lin and Lee*, 1995]. Consistent with the observations, we study how the reconnection outflow develops in a 3-D model with a finite x-line by imposing a spatially localized region of reconnected flux B_z on top of a Harris current sheet. A particle-in-cell (PIC) model is used so that the collisionless dissipation of reconnection-driven flows can be studied. The system is initially in pressure balance, but the curvature forces that drive reconnection are not balanced by any other forces and drive the outflow.

We explore a system periodic in three directions: with x-z the plane of reconnection and the reconnection outflow along x. Superimposed on a double Harris current layer $B_x(z)$ with a half width of $2.0d_i$ (with d_i the ion inertial length) is a region of uniform magnetic flux $B_z(x, y)$ that is localized with a width of $8.0d_i$ in the x-y plane as shown in Figure 1a. There is no ambient guide field. The density in the region of $B_z \neq 0$ is equal to the background density n_0 of the Harris system. The electron and ion temperatures are adjusted so that the total pressure is balanced with $T_i/T_e = 5$, which is typical for the magnetosphere. Required currents are carried by both species, in proportionality to their temperature. Unbalanced forces associated with magnetic tension will drive the plasma in the region of $B_z \neq 0$ to the left in Figure 1a. The motion of the plasma in the second current sheet is essentially identical but in the opposite direction is and not discussed further. The results of our PIC simulations are presented in normalized units: the magnetic field to the asymptotic value B_0 of the Harris reversed field, the density to the value at the center of the current sheet minus $n_0 = 0.3$, velocities to the Alfvén speed c_A, lengths to d_i, times to the inverse ion cyclotron frequency Ω_{ci}^{-1}, and temperatures to $m_i c_A^2$. The computational domain is $102.4d_i \times 25.6d_i \times 25.6d_i$. Other parameters of the simulations are a mass ratio $m_i/m_e = 25$, which is sufficient to separate the dynamics of the two species [*Hesse et al.*, 1999], and speed of light $c = 15c_A$.

Shown in Figure 1 is B_z in the center of the current sheet ($z = 0$) at (a) $t = 0$, (b) $t = 12\Omega_{ci}^{-1}$, and (c) $t = 24\Omega_{ci}^{-1}$. The outflow carries the flux B_z to the left propelled by the unbalanced magnetic curvature forces that drive reconnection. The electron and ion flows in the x-y plane at $t = 30\Omega_{ci}^{-1}$ are shown in Figures 2a–2d. Both species flow to the left in the core of the jet as expected. The strong electron flows at the boundaries of the jet produce a counterclockwise current loop that is the dominant source of the magnetic field B_z shown in Figure 1. A surprise in this data is the strong positive ion flow just below the main flow in a region where $B_z \sim 0$, and there is therefore no curvature. The reason for this flow is discussed later. In the core of the flow jet the flux B_z is carried upward in Figure 1, which is in the electron drift direction (Figure 2c), and is compressed at the upper edge. In contrast, the left edge of the jet turns downward, which is in the ion drift direction (Figure 2d). Similar turning in the ion drift direction was seen in 3-D PIC simulations of interchange turbulence in the magnetotail [*Pritchett and Coroniti*, 2013]. The downward motion of electrons at the front of the jet in Figure 2c, which is opposite to their drift in the initial current layer, is due to an $\mathbf{E} \times \mathbf{B}$

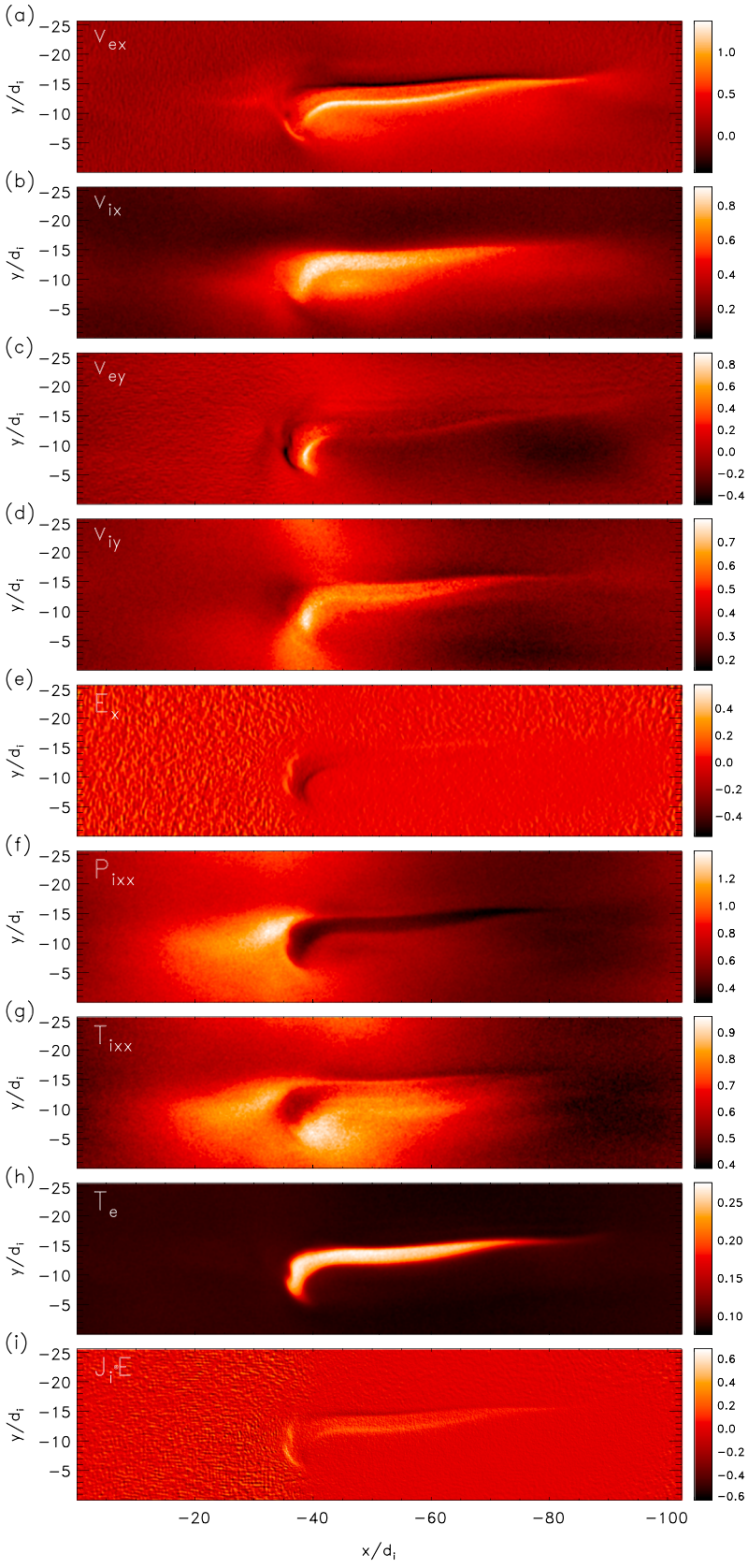

Figure 2. As in Figure 1 at $t = 30\Omega_{ci}^{-1}$ plots of (a) v_{ex}, (b) v_{ix}, (c) v_{ey}, (d) v_{iy}, (e) E_x, (f) p_{ixx}, (g) T_{ixx}, (h) T_e, and (i) the ion heating rate $\mathbf{J}_i \cdot \mathbf{E}$.

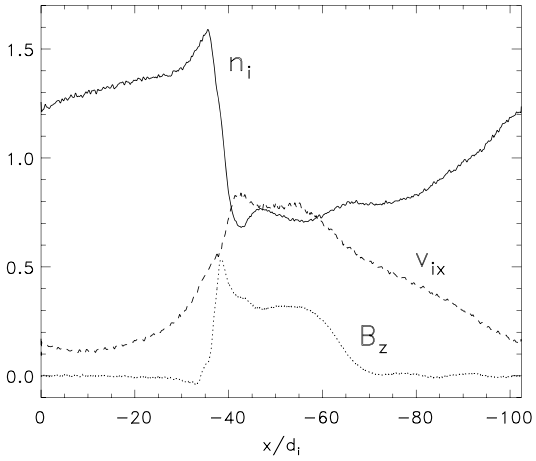

Figure 3. Cuts of the ion density n_i (solid), v_{ix} (dashed), and B_z (dotted) along x at $z = 0$ and $y = -11.3d_i$ at the same time as in Figure 2.

drift from an electric field E_x directed to the right (Figure 2e). For ions this drift adds to their ambient downward flow (Figure 2d). The asymmetry of the structure of the jet in the y direction is contrasted with the results of an MHD simulation with nearly identical initial conditions in which the jet forms a symmetrical structure in the x-y plane (Figure 1d). These MHD flows are similar to those from earlier 3-D MHD simulations of plasma interchange-driven flows in the magnetotail [*Birn et al.*, 2004]. The direction and magnitude of the deflections of the front will likely depend on the width of the initial Harris current layer, which controls the magnitude of the initial ion drift speed. A broader initial current layer will lead to deflections in both directions, closer to that seen in the MHD model. Note also that the net displacement along x in the present simulations is far smaller than seen in the satellite data, which is a limitation of the size of the simulation.

In Figure 3 are cuts of the ion density (solid), B_z (dotted), and the ion velocity v_{ix} (dashed) versus x in the center of the current sheet at $t = 24\Omega_{ci}^{-1}$. The density drops sharply across the front and into the jet although the density minimum of around 0.7 is well above the initial condition of 0.3. B_z rises sharply across the front and exhibits the distinctive dip and overshoot that are often seen in the observations [*Ohtani et al.*, 2004; *Runov et al.*, 2009]. The overshoot results from local compression at the front, which produces a similar peak in the density. The region of negative B_z ahead of the front can also be seen as the white region in Figure 1c in the interval $-35d_i < x < -25d_i$ and $-9d_i > y > -13d_i$. The mechanism for this reversal in B_z appears to be similar to the self-generation of magnetic fields in the Weibel instability and will be discussed more fully in a separate publication.

The ion velocity rises gradually ahead of the front as in observations and reaches a plateau around $0.8c_A$, which is well below that expected based on the upstream Alfvén speed ($1.8c_A$). The velocity v_f of the front is around $0.46c_A$ and is calculated by stacking cuts of B_z versus x at several times (Figure 4). The reduced velocity of the front compared with that of the core of the jet results from the buildup of ion pressure ahead of the front shown in Figure 2f. The increase in pressure is largest at the top corner of the front and serves to both slow the jet and deflect it downward. Such pressure enhancements have been documented in satellite measurements [*Liu et al.*, 2013]. The pressure increase is a consequence of the reflection of ions in the current sheet off of the head of the front, which has also been documented in satellite observations [*Zhou et al.*, 2010] and discussed in 2-D reconnection models [*Wu and Shay*, 2012]. The penetration of high-velocity ions in the jet through the front also contributes to the pressure increase. Both classes of particles can be seen to the left of the front in the $x - v_x$ phase space in Figure 5a, which is from the center of the current sheet with $y = -11.8d_i$ and $t = 20\Omega_{ci}^{-1}$. The cut of B_z in Figure 5b shows the location of the front. As expected, the reflected ions have a velocity close to c_A, which is around twice v_f. In Figure 2g is the ion temperature T_{ixx} corresponding to the pressure in Figure 2f. The increase in ion temperature associated with the reflected ions is evident. The rate of ion heating $\mathbf{J}_i \cdot \mathbf{E}$ is shown in Figure 2i. Ion

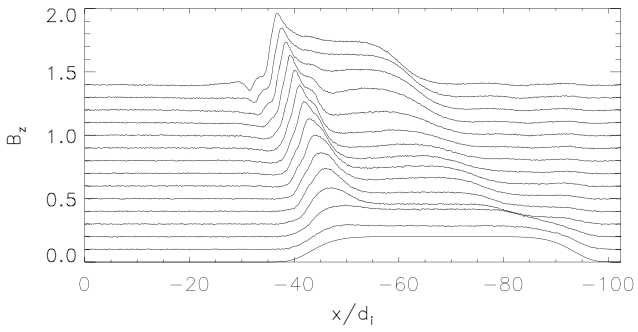

Figure 4. A stack of cuts of B_z along x at $z = 0$ and $y = -11.3d_i$ separated by time intervals of $2\Omega_{ci}^{-1}$ starting from $t = 0$. The velocity of the front calculated from the peaks of B_z is $0.46c_A$.

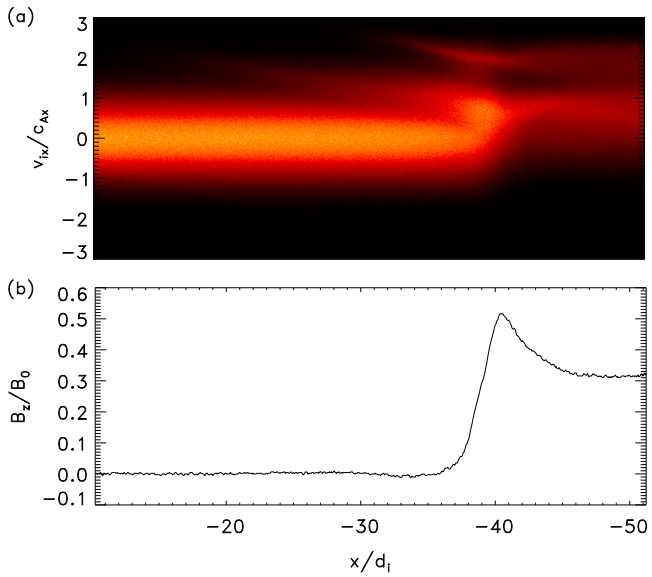

Figure 5. In (a) the ion phase space $v_x - x$ in the center of the current sheet at $y = -11.3d_i$ and $t = 20\Omega_{ci}^{-1}$. In (b) a cut of B_z at the same time and location.

heating peaks at the front, at the lower boundary of the exhaust and in turbulent fluctuations in a broad region ahead of the front. The source of these fluctuations has not been explored.

The mechanism that produces the enhanced ion temperature below the jet and to the right of the front is also responsible for the strong leftward directed flow in the same region shown earlier in Figure 2b. Ions moving to the left in the core of the jet also drift downward (Figure 2d) and eventually exit the region of strong B_z into the adjacent stationary plasma. These ions continue to flow to the left through the stationary background ions. The resulting counterstreaming ion velocity distributions in this region where $B_z \sim 0$ have a net drift to the left (Figure 2b) and produce an effective T_{ixx} as seen in Figure 2g. A cut along x at $y = -10d_i$ (not shown) reveals a localized peak in B_z at the front but with a flow to the left that remains large well to the right of the front where $B_z \sim 0$. Such behavior has been documented in THEMIS spacecraft magnetotail observations [*Runov et al.*, 2011b]. In contrast with the ions, we have measured no significant increase in the electron temperature at the front (Figure 2h) in spite of the intense electron current in the x-y plane that produces the rather complex magnetic structure B_z in Figure 1.

Before further addressing the properties of the front, we emphasize that this sharp boundary is not a shock. First, in the upstream region to the right of the front the fast-mode phase speed based on the total plasma and magnetic pressure is around $1.0c_A$ while the flow speed of the jet is around $0.8c_A$, so the upstream Mach number is less than unity. Further, if the front were a shock, the flow through the shock would carry the flux B_z across the shock into the downstream region, which is not seen in the simulation data. Nevertheless, while the front is not a shock, that the velocity in the core of the flow burst is substantially higher than that of the front has important implications for understanding the dissipation of reconnection driven flows. The plasma within the jet eventually catches up to the front where it is compressed and deflected with reduced velocity downward in Figure 2d. The consequence is that the integrated volume of plasma behind the flow burst (measured by the reduction in the size of the nonzero B_z region) decreases with time. This can be seen in Figures 1b and 1c. The integrated magnetic flux B_z in the jet is decreasing with time and the corresponding flux convecting downward is increasing (Figure 1). Thus, the front is more than simply the front edge of the jet. Rather, it is the site for conversion of flow energy into ion thermal energy and much of the plasma that makes up the jet will be directly processed within the front.

A simple analytic calculation illustrates how the reduction in flow energy takes place. We consider a simple 2-D system in the x-y plane in which the plasma in the current sheet (density n_{cs}) interacts with the plasma in the jet (density n_b). The front and jet velocities are v_f and v_b, respectively, while the current sheet ions are at rest. For simplicity, we ignore the ambient drift along y, which adds complexity to the calculation but does not change the final result. In the frame of the front, ions in the current sheet that move with a velocity $-v_f$ along x are reflected by the magnetic boundary and leave the front with a velocity v_f. The jet ions have an incident velocity $v_b - v_f$ and are deflected into the y direction with their speed unchanged. Force balance at the front, neglecting the residual magnetic stress, yields $2n_{cs}v_f^2 = n_b(v_b - v_f)^2$, which can be solved for the front velocity $v_f = Rv_b/(1 + R)$ where $R = \sqrt{n_b/2n_{cs}}$. In the frame of the front, neither the current sheet nor the jet ions change energy. In the simulation frame, however, there is a transfer

of energy from the jet ions to the current sheet ions. The change in energy $\Delta W = W_f - W_i$ of the jet ions is given by

$$\Delta W = \frac{1}{2} m_i n_b \left(v_f^2 + (v_b - v_f)^2 - v_b^2 \right) = -2W_i \frac{R}{(1+R)^2} \quad (1)$$

with $W_i = m_i n_b v_b^2/2$. This energy loss corresponds to the energy gain of the current sheet ions. Thus, the fraction of energy conversion is linked to the density ratio between the jet and current sheet ions. In the limit of $n_b/n_{cs} \to 0$ there is no energy conversion. For a typical value $n_b/n_{cs} = 0.2$ [*Runov et al.*, 2009] the fraction of energy conversion is 0.37 according to this simple model. The model, of course, greatly simplifies a very complex system. The model prediction of the front velocity in the simulation is $0.3c_A$ compared with the measured value of $0.46c_A$.

Finally, we emphasize that neither the deflection of the jet into the y direction nor the reduced velocity of the front compared with the jet have can take place in a 2-D reconnection model. In a 2-D model therefore, the core of the jet does not cycle through the front as in the 3-D model. Estimates of the front velocity based on multispacecraft THEMIS observations have been presented [*Runov et al.*, 2011a], but a direct comparison with the velocity of the core of the jet has not been carried out. This comparison would be facilitated if a local measure of the velocity of the front from single-spacecraft data could be obtained. From the simulation we have evaluated the local $\mathbf{E} \times \mathbf{B}$ velocity at the peak of B_z. At $t = 30\Omega_{ci}^{-1}$ this velocity is $0.47c_A$, which is quite close to the value of $0.46c_A$ deduced from the stack of plots in Figure 4. The local ion velocity v_{ix} at the peak of B_z is also close to but somewhat higher than the front velocity.

The overshoot in B_z seen in many observations of RJF encounters in the magnetotail is already evidence of the pileup of the jet plasma at the front, but direct comparisons of the front velocity with that of the core of the jet are necessary to test the ideas presented here. While the focus of the present paper is on reconnection-driven jets, jets driven by the magnetized Rayleigh-Taylor instability [*Birn et al.*, 2004] or other mechanisms might also exhibit similar deflections and associated dissipation of bulk flow energy.

Acknowledgments

The authors would like to thank V. Angelopoulos, A. Runov, and L.S. Shepherd for helpful discussions. This work was supported in part by NASA grants NNX14AC78G, NNX08AO83G, and NNX10AN08A and NSF grant AGS-093463. Computations were performed at the National Energy Research Scientific Computing Center and on NASA Advanced Supercomputing Division resources. Because of the large storage requirements of the data from the simulations (around a terabyte), the data are not publicly available.

The Editor thanks Stefan Eriksson and an anonymous reviewer for their assistance in evaluating this paper.

References

Angelopoulos, V., et al. (1997), Magnetotail flow bursts: Association to global magnetospheric circulation, relationship to ionospheric activity and direct evidence for localization, *Geophys. Res. Lett.*, *24*(18), 2271–2274.

Angelopoulos, V., A. Runov, X.-Z. Zhou, D. L. Turner, S. A. Kiehas, S.-S. Li, and I. Shinohara (2013), Electromagnetic energy conversion at reconnection fronts, *Science*, *341*, 1478–1482.

Birn, J., J. Raeder, Y. Wang, R. Wolf, and M. Hesse (2004), On the propagation of bubbles in the geomagnetic tail, *Ann. Geophys.*, *22*, 1773–1786, doi:10.5194/angeo-22-1773-2004.

Cassak, P. A., J. F. Drake, J. T. Gosling, T. Phan, M. A. Shay, and L. S. Shepherd (2013), On the cause of supra-arcade downflows, *Astrophys. J. Lett.*, *775*, L14, doi:10.1088/2041-8205/775/1/L14.

Gosling, J. T., R. M. Skoug, and D. J. McComas (2005), Direct evidence for magnetic reconnection in the solar wind near 1 AU, *Geophys. Res. Lett.*, *110*, A01107, doi:10.1029/2004JA010809.

Hesse, M., K. Schindler, J. Birn, and M. Kuznetsova (1999), The diffusion region in collisionless magnetic reconnection, *Phys. Plasmas*, *5*, 1781.

Hoshino, M., T. Mukai, and T. Yamamoto (1998), Ion dynamics in magnetic reconnection: Comparison between numerical simulation and Geotail observations, *J. Geophys. Res.*, *103*, 4509–4530.

Hoshino, M., T. Mukai, T. Terasawa, and I. Shinohara (2001), Suprathermal electron acceleration in magnetic reconnection, *J. Geophys. Res.*, *106*, 25,979–25,997.

Lin, Y., and L. C. Lee (1995), Simulation study of the Riemann problem associated with magnetotail reconnection, *J. Geophys. Res.*, *100*, 19,227–19,237.

Linton, M. G., and D. W. Longcope (2006), A model for patchy reconnection in three dimensions, *Astrophys. J.*, *642*, 1177–1192, doi:10.1086/500965.

Liu, J., V. Angelopoulos, X.-Z. Zhou, A. Runov, and Z. Yao (2013), On the role of pressure and flow perturbations around dipolarizing flux bundles, *J. Geophys. Res. Space Physics*, *118*, 7104–7118, doi:10.1002/2013JA019256.

Masuda, S., T. Kosugi, H. Hara, S. Tsuneta, and Y. Ogawara (1994), A loop-top hard x-ray source in a compact solar flare as evidence for magnetic reconnection, *Nature*, *373*, 495–497.

McKenzie, D. E., and H. S. Hudson (1999), X-ray observations of motions and structurte above a solar flare arcade, *Astrophys. J. Lett.*, *519*, L93–L96.

Nakamura, R., et al. (2004), Spatial scale of high-speed flows in the plasma sheet observed by Cluster, *Geophys. Res. Lett.*, *31*, L09804, doi:10.1029/2004GL019558.

Ohtani, S.-I., M. A. Shay, and T. Mukai (2004), Temporal structure of the fast convective flow in the plasma sheet: Comparison between observations and two-fluid simulations, *J. Geophys. Res.*, *109*, A03210, doi:10.1029/2003JA010002.

Petschek, H. E. (1964), Magnetic Field Annihilation, in *AAS/NASA Symposium on the Physics of Solar Flares*, edited by W. N. Ness, pp. 425–439, NASA, Washington, D. C.

Pritchett, P. L., and F. V. Coroniti (2013), Structure and consequences of the kinetic ballooning/interchange instability in the magnetotail, *J. Geophys. Res. Space Physics*, *118*, 146–159, doi:10.1029/2012JA018143.

Runov, A., V. Angelopoulos, M. I. Sitnov, V. A. Sergeev, J. Bonnell, J. P. McFadden, D. Larson, K.-H. Glassmeier, and U. Auster (2009), THEMIS observations of an earthward-propagating dipolarization front, *Geophys. Res. Lett.*, *36*, L14106, doi:10.1029/2009GL038980.

Runov, A., V. Angelopoulos, X.-Z. Zhou, X.-J. Zhang, S. Li, F. Plaschke, and J. Bonnell (2011a), A THEMIS multicase study of dipolarization fronts in the magnetotail plasma sheet, *J. Geophys. Res.*, *116*, A05216, doi:10.1029/2010JA016316.

Runov, A., et al. (2011b), Dipolarization fronts in the magnetotail plasma sheet, *Planet. Space Sci.*, *59*, 517–525, doi:10.1016/j.pss.2010.06.006.

Sitnov, M. I., M. Swisdak, and A. V. Divin (2009), Dipolarization fronts as a signature of transient reconnection in the magnetotail, *J. Geophys. Res.*, *114*, A04202, doi:10.1029/2008JA013980.

Sonnerup, B. U. Ö., G. Paschmann, I. Papamastorakis, N. Sckopke, G. Haerendel, S. J. Bame, J. R. Asbridge, J. T. Gosling, and C. T. Russell (1981), Evidence for magnetic field reconnection at the Earth's magnetopause, *J. Geophys. Res.*, *86*, 10,049–10,067.

Wu, P., and M. A. Shay (2012), Magnetotail dipolarization front and associated ion reflection: Particle-in-cell simulations, *Geophys. Res. Lett.*, *39*, L08107, doi:10.1029/2012GL051486.

Zhou, X.-Z., V. Angelopoulos, V. A. Sergeev, and A. Runov (2010), Accelerated ions ahead of earthward propagating dipolarization fronts, *J. Geophys. Res.*, *115*, A00I03, doi:10.1029/2010JA015481.